Toluene PLIF thermometry and imaging in supersonic flows

By V. A. Miller, M. Gamba, M. G. Mungal AND R. K. Hanson

1. Motivation and objectives

This work is motivated by a need for flowfield characterization in high-speed, compressible flows. Toluene planar laser-induced fluorescence (PLIF) has been identified as a well-suited diagnostic to satisfy this need.

PLIF has been utilized with various tracers in gas- and liquid-phase for a variety of quantitative measurements, including thermometry, mixture-fraction imaging, and fuel-to-air ratio imaging in a number of applications (Schulz & Sick 2005). Of the various gaseous tracers available, toluene has been identified as a tracer with unique photophysical properties (Burton & Noyes 1968): the fluorescence signal of toluene is strongly quenched by oxygen, and therefore makes it well-suited for fuel-to-air imaging (Koban *et al.* 2005*a*); and its high quantum yield and strong sensitivity to temperature below $900K$ (Koban *et al.* 2004) also make it well-suited for thermometry. This latter property makes toluene-based PLIF strategies particularly attractive for the study of supersonic flows, where large temperature discontinuities and gradients exist within the flowfield. For example, toluene PLIF was recently demonstrated in supersonic flows to identify the structure of a shock/boundary layer interaction Yoo *et al.* (2010).

However, the low vapor pressure of toluene below room temperature conditions, and the high sensitivity to oxygen limit its implementation in many supersonic flow facilities. Traditional supersonic wind tunnels predominantly use air as the working fluid and are operated at low ($\sim 100K$) static temperatures and pressures. These conditions make the use of toluene impractical or not possible.

On the contrary, impulse facilities, such as shock tubes, shock tunnels, and expansion tubes, are ideal for the use of toluene as a tracer species in supersonic, low- to moderate-enthalpy flows. In particular, an expansion tube gives flexibility on the choice of test gas and access to a broad range of static conditions thus making the use of toluene attractive for the study of compressible flow phenomena.

In this work, the developments of toluene PLIF toward a robust technique for thermometry imaging in supersonic flows in short-duration impulse facilities are reported. First, a theoretical treatment of single- and dual-band LIF collection strategies are presented; in particular, sensitivity and accuracy of each strategy are assessed. It is shown that single-band toluene LIF collection can be used directly as a temperature diagnostic in uniform pressure flowfields, whereas dual-band collection strategies can be used to measure temperature in variable pressure flowfields.

Lastly, single-band LIF imaging is demonstrated on two canonical compressible flow configurations: supersonic flow over a 20° wedge and around a cylinder. Supersonic flow over a wedge is used to demonstrate single-band toluene thermometry in constant-pressure conditions, where calibration is inferred from a measure of the LIF signal across the oblique shock over the wedge. Flow around a cylinder is used to demonstrate single-band collection as an effective visualization tool. For the time being, in preparation of

future work on dual-band detection, the results of single-band imaging of flow around the cylinder are assessed against synthetic LIF signals computed from 2D RANS calculations of the same configuration.

2. Single- and dual-band collection strategies

Laser-induced fluorescence (LIF) is a two step process: first, a species is excited to an upper quantum state via absorption of radiation; second, the species spontaneously relaxes back to its ground state by fluorescing. The resulting LIF signal S_f is described by the LIF equation, which is the product of the number of incident photons $\frac{E}{h\nu}$ on the field of view, the number density of the absorbing species n, the absorption cross section σ, the fraction of photons that are re-emitted as fluorescence ϕ (known as the fluorescence quantum yield, FQY), and an optical collection efficiency factor η

$$S_f = \frac{E}{h\nu} n\sigma(\lambda, T)\phi(\lambda, T, P_i)\eta. \tag{2.1}$$

Equation 2.1 applies under linear excitation regime (i.e., negligible stimulated emission of fluorescence) and when photoionization and predissociation are negligible. The photophysical parameters σ and ϕ depend on local temperature T and partial pressure P_i of the absorbing and bath species, and excitation wavelength λ. Knowledge of how these parameters varies with T, P_i, and λ allows for the inference of T or P_i using specific excitation and/or fluorescence collection strategies, which are typically based on ratiometric approaches where ratios of LIF signals are used to simplify equation 2.1.

Two single-wavelength excitation strategies are considered in this work: single- and dual-band fluorescence collection. Typically, the single-band collection strategy images fluorescence from a single region of the emission spectrum and, in uniform pressure regions, uses information of the value of temperature at one point to infer the temperature elsewhere (Koch 2005; Yoo *et al.* 2010). In the wedge flow we assume that such information is not available in the experiment and, therefore, a different method based on a measure of the flow Mach number from the shock angle is used to reduce Equation 2.1.

The dual-band collection strategy employs two cameras to collect fluorescence from two different regions of the emission spectrum using optical filters. Under the assumption that σ and ϕ are solely a function of temperature (i.e., pressure effects are negligible on the photophysics of toluene), temperature is directly inferred by taking the ratio of these two images.

The strategies presented above can be optimized only if details of the photophysical parameters are known. Toluene absorption is centered around 265 nm (Koban *et al.* 2004), and is accessible by commercially available KrF excimer lasers (248 nm) and frequency quadrupled Nd:YAG lasers (266 nm). The absorption cross section at 266 nm increases with increasing temperature, however, σ is approximately constant for 248 nm excitation (Figure 1a). Furthermore, toluene FQY decreases steeply for both 248 nm and 266 nm excitation, dropping three orders of magnitude for both excitation wavelengths over the temperature range considered (Figure 1b).

Koban *et al.* (2004) has characterized photophysical parameters of toluene from 298 K to 900 K and at 1 bar total pressure in nitrogen. Furthermore, the FQY of toluene remains constant at pressures above 1 bar for both 248 nm excitation (Yoo *et al.* 2010) and 266 nm excitation (Cheung 2011) at room temperature. The single-band and dual-band collection strategies presented in this work are constructed under the assumptions that

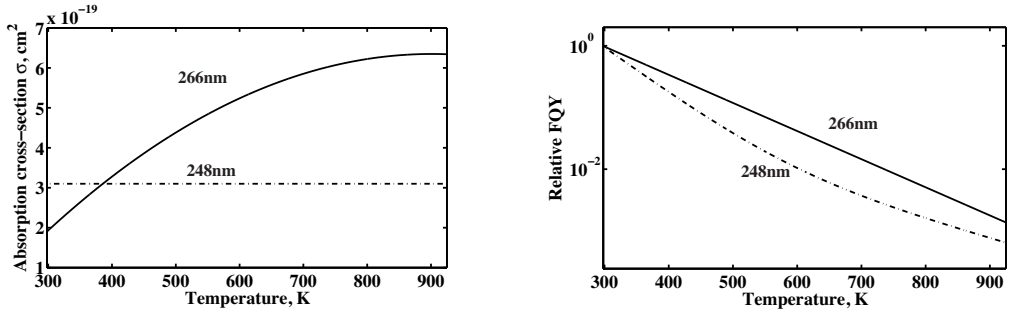

(a) (b)

FIGURE 1. Photophysical parameters σ (a) and ϕ (b) of toluene for 266 nm and 248 nm excitation. Curves for σ with 266 nm excitation are fit through measurements by Koban *et al.* (2004), whereas σ for 248 nm excitation is taken to be approximately constant, as is done by Koban *et al.* (2004).

oxygen quenching is absent (this work is done in nitrogen, in which collisional quenching is negligible) and the FQY of toluene is independent of toluene partial pressure (i.e., pressure is greater than 1 bar) even at high temperatures. The limited information available from previous work and theoretical considerations supports the latter assumption (Koban *et al.* 2004; Yoo *et al.* 2010; Cheung 2011).

2.1. *Single-band collection thermometry across an oblique shock*

Yoo *et al.* (2010) has demonstrated single-band toluene PLIF thermometry and visualization of shock tube flows. Yoo *et al.* made quantitative temperature measurements in uniform pressure fields by acquiring a calibration image at known uniform conditions, subsequently acquiring an image of the flow of interest, and then taking the ratio of these two images to solve for temperature T (assuming ϕ is not a function of pressure P_i, and P_i is uniform in the region being analyzed):

$$\frac{S_f}{S_{fcal}} = \frac{n\sigma(\lambda,T)\phi(\lambda,T)}{n_{cal}\sigma(\lambda,T_{cal})\phi(\lambda,T_{cal})} = \frac{P_i T_{cal}}{T P_{ical}} \frac{\sigma(\lambda,T)\phi(\lambda,T)}{\sigma(\lambda,T_{cal})\phi(\lambda,T_{cal})}. \tag{2.2}$$

For calculation of temperature T, this strategy requires knowledge of the number density n, or T_{cal}, P_{cal}, and P_i for both the calibration image and the test-image.

When this calibration approach is not possible or the number density of the tracer is not known, temperature can be inferred by applying some other condition. One possible approach we propose is to use a measure of the LIF signal ratio across an oblique shock S_{fu}/S_{fd} at a given incoming flow Mach number (where subscripts u and d are for upstream and downstream, respectively), to infer temperature:

$$\frac{S_{fu}}{S_{fd}} = \frac{P_{iu}}{P_{id}} \frac{T_d}{T_u} \frac{\sigma(\lambda,T_u)\phi(\lambda,T_u)}{\sigma(\lambda,T_u\frac{T_d}{T_u})\phi(\lambda,T_u\frac{T_d}{T_u})}. \tag{2.3}$$

By measuring the shock angle β from the PLIF image and knowing the turning angle θ, one can infer the Mach number M and eliminate the pressure ratio P_{iu}/P_{id} and temperature ratio T_d/T_u in Equation 2.3. Using ideal oblique-shock relations, Equation 2.3 becomes only a function of Mach number M and T_u

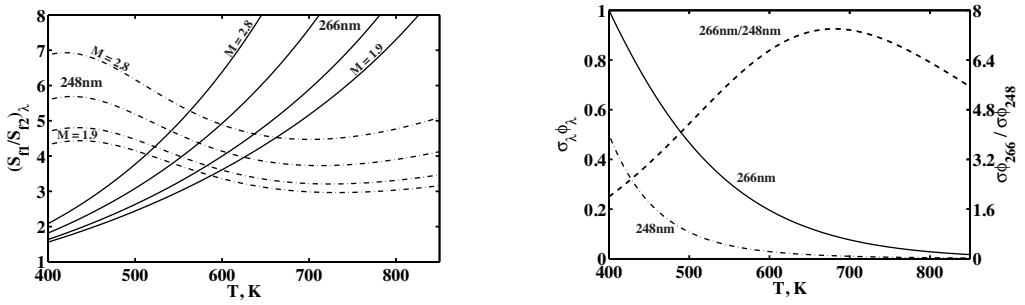

(a) (b)

FIGURE 2. (*a*) Expected signal ratio across an oblique shock with turning angle $\theta = 20°$ for 248 nm (*dash-dot*) and 266 nm (*solid*) excitation and for Mach number 1.9 2.3, 2.5, and 2.8. (*b*) Relative expected signals upstream of the shock for 248 nm (*dash-dot*) and 266 nm (*solid*) excitation on the left ordinate. The ratio of these expected signals (*dotted*) is on the right ordinate.

$$\frac{S_{fu}}{S_{fd}} = g(M)f(M)\frac{\sigma(\lambda, T_u)\phi(\lambda, T_u)}{\sigma(\lambda, T_u f(M))\phi(\lambda, T_u f(M))}, \tag{2.4}$$

where $g(M)$ and $f(M)$ are ideal relations for pressure ${}^{P_d}/_{P_u}$ and temperature ${}^{T_d}/_{T_u}$ ratios across an oblique shock.

By assuming a range of flow Mach number M and temperature T_u that are accessible by the Stanford Expansion Tube Facility, we can calculate the expected signal ratios for both 266 nm and 248 nm excitation as a function of temperature and Mach number. By taking the derivative of the curves in Figure 2a (not shown), we see that 248 nm and 266 nm excitation exhibit similar temperature sensitivity for $T_u \sim 500$ K (the targeted upstream temperature, see section 3.1) using this thermometry strategy. Generally, expected signal ratios increase with increasing Mach number, consistent with the increase in temperature ratio across a shock for increasing Mach number.

Note that Equation 2.4 is applicable only across an ideal oblique shock, immediately upstream and downstream of the shock; this thermometry strategy also assumes that the flow field is uniformly seeded with tracer (i.e., $\frac{n_{iu}}{n_{id}} = \frac{P_{iu}}{P_{id}}\frac{T_d}{T_u}$). Under these assumptions, Equation 2.4 gives a closed form relationship between T_u and the locally measured M and ${}^{S_{fu}}/_{S_{fd}}$.

A mean signal ratio $\overline{{}^{S_{fu}}/_{S_{fd}}}$, mean upstream signal $\overline{S_{fu}}$, and mean upstream temperature $\overline{T_u}$ are computed by taking values along the length of the shock. Using these values for $\overline{S_{fu}}$ and $\overline{T_u}$, the rest of the image is converted to temperature using Equation 2.2 by substituting S_{fcal} and T_{cal} with $\overline{S_{fu}}$ and $\overline{T_u}$, where ${}^{P_i}/_{P_{ical}}$ is either unity in the upstream region or $f(M)$, the pressure ratio across the ideal shock, in the downstream region.

For this collection strategy, both 266 nm and 248 nm excitation sources can be used. At a given temperature, LIF signals are proportional to the product of absorption cross section and FQY

$$S_f \propto \sigma(\lambda, T)\phi(\lambda, T). \tag{2.5}$$

Neither 266 nm nor 248 nm exhibit substantially more temperature sensitivity near $T_u = 500$ K; additionally, the larger absorption cross-section and greater FQY with 266 nm excitation near 500 K (Figure 1a) results in LIF signals up to seven times greater

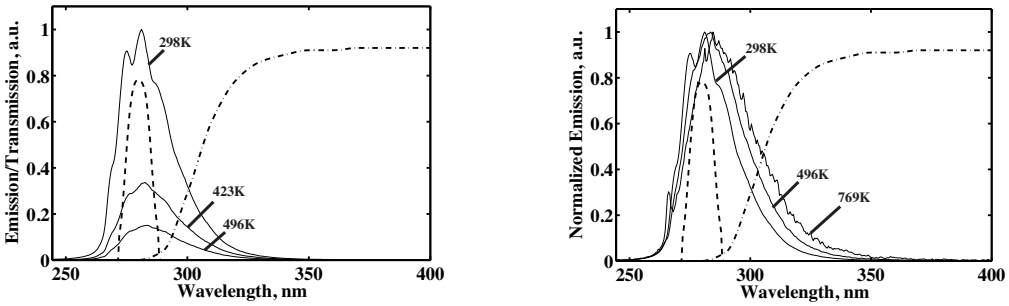

(a) (b)

FIGURE 3. (*a*) Toluene emission spectra normalized to peak emission at 298 K. Spectra shown were measured at 1 bar total pressure in nitrogen. WG280 (*dash*) and BP280 (*dash-dot*) transmission curves are overlaid. (*b*) Toluene emission spectra normalized to maximum signal for each temperature to illustrate the change in relative signal magnitude as a function of wavelength and temperature. (Data courtesy of J. D. Koch and W. Koban.)

than those expected with 248 nm excitation (Figure 2b). Therefore, we elect to use 266 nm excitation to maximize LIF signal. Note that we did not exercise turning angle θ in our calculation of expected signal ratios S_{f1}/S_{f2}, which may yield different strategies.

2.2. *Dual-band collection strategies*

Koban *et al.* (2004) has shown that the emission spectrum of toluene redshifts with increasing temperature for both 248 nm and 266 nm excitation. This redshift enables dual-band collection thermometry; by using two cameras to simultaneously collect fluorescence from different regions of the spectrum following single-wavelength excitation, one can infer temperature by taking the ratio of these two images. For pressures above 1 bar, we assume ϕ does not depend on partial pressure; therefore, the ratio of two images (subscripts 1 and 2) for which different portions of the spectrum are collected is only a function of temperature,

$$\frac{S_{f1}}{S_{f2}} = \frac{[\phi(\lambda,T) * F_1(\lambda)]\eta_1}{[\phi(\lambda,T) * F_2(\lambda)]\eta_2}, \tag{2.6}$$

where $[\phi(\lambda,T) * F(\lambda)]$ is the convolution of the FQY with an optical filter transmission curve. The efficiencies η are not eliminated from the equation in order to account for collection efficiencies and response of the two cameras. However, other requirements of single-band collection (i.e., uniform tracer number density, excitation laser fluence, absorption) are eliminated.

This dual-band collection has been theoretically studied in the past by Koban *et al.* (2004) using a variety of filters available from Schott Glass, and recently demonstrated by Mohri *et al.* (2011) to image O_2 concentration using 248 nm excitation. In this work, we propose to use high-transmission ($\sim 80\%$), narrow-band (10 nm) band-pass interference filters (in the range $260 - 320$ nm) combined with Schott glass filters to further optimize the method. One promising combination identified in the study uses an interference filter centered at 280 nm and a long-pass Schott glass filter (WG320) to construct the temperature calibration curve. The result of this combination, shown in Figure 4, offers sensitivity similar to the 266 nm excitation single-band collection strategy shown in Figure 2a.

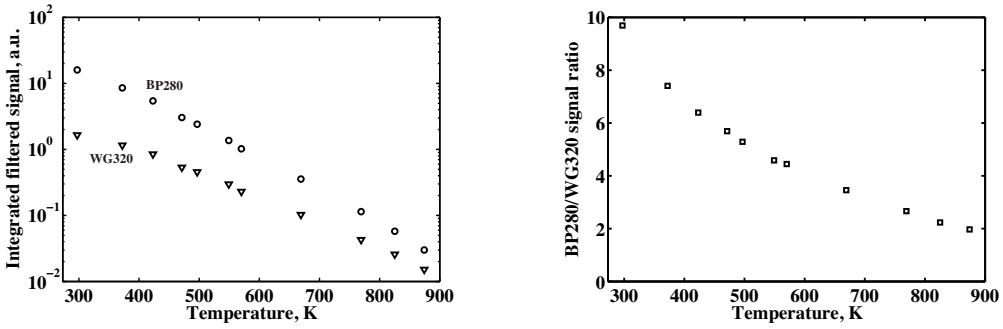

(a) (b)

FIGURE 4. (*a*) Expected signals as a function of temperature using a band-pass filter centered at 280 nm (*open circles*, BP280) and a Schott Glass WG320 long-pass filter (*open triangles*). (*b*) Ratio of expected signals from (*a*)

Emission spectra resulting from 266 nm excitation are used to calculate temperature calibration curves. Emission spectra using 248 nm excitation have similar qualitative shapes (Koban *et al.* 2005*b*). As shown in Figure 2b, 248 nm excitation LIF signals are several times smaller due to toluene's smaller absorption cross section with 248 nm excitation and lower FQY near $T = 500$ K; to maximize signal levels, we consider only 266 nm excitation for dual-band collection.

2.3. *Uncertainty propagation for single- and dual-band thermometry*

After describing the single-wavelength excitation with single- and dual-band collection, we now investigate the expected accuracy of each method by conducting an error propagation study. In practice, toluene LIF signals are acquired using an ICCD camera, which is inherently noisier than a CCD camera. The LIF signals are then converted to temperature using one of the strategies described above. We define the signal to noise ratio SNR, a measure of relative uncertainty in the signal, as the average signal $\overline{S_f}$ divided by the root-mean-square of the signal σ_f for an n by m pixel region of the image, under the assumption that the flow field is uniform through the interrogation window. For the thermometry strategies described above, uncertainty in temperature can be quantified via linearized error propagation:

$$dT^2 = \left(\frac{dT}{dS_{f1}}\right)^2 \sigma_{f1}^2 + \left(\frac{dT}{dS_{f2}}\right)^2 \sigma_{f2}^2, \tag{2.7}$$

which can be reduced to

$$dT^2 = \left(\frac{dT}{d\psi}\right)^2 \left(\frac{S_{f1}}{S_{f2}}\right)^2 \left(\frac{1}{SNR_1^2} + \frac{1}{SNR_2^2}\right), \tag{2.8}$$

where $\psi = {}^{S_{f1}}/_{S_{f2}}$, either for the signal ratio across an oblique shock in single-band collection or for the signal ratio of the two images in dual-band collection.

Using Equation 2.8, we compute uncertainties in temperature for the single- and dual-band imaging scheme as a function of temperature for different values of SNR. A third-order polynomial is fit to temperature calibration curves (Figures 2a and 4b) and ana-

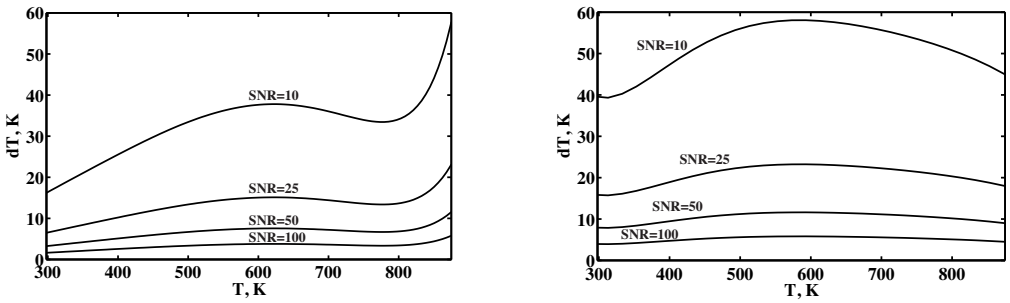

FIGURE 5. Temperature accuracy for single- (*a*) and dual-band (*b*) fluorescence collection thermometry

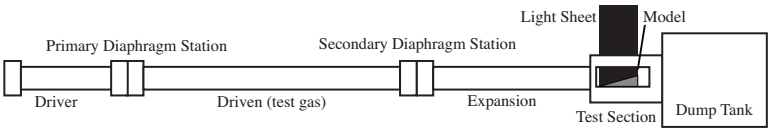

FIGURE 6. Schematic of Stanford Expansion Tube Facility. Tube is 14 cm in inner-diameter and 12 m long from driver to test section.

lytically differentiated to compute $\frac{dT}{d\psi}$. For simplicity, SNR_1 is assumed to be equal to SNR_2.

Uncertainty in temperature dT is shown in Figure 5 as a function of temperature and SNR for single-band thermometry and dual-band thermometry over a range of SNR values.

We find a similar magnitude of uncertainty in temperature dT as a function of SNR and temperature T for both the BP280/WG320 dual-band scheme and single-band oblique shock thermometry. We deem it reasonable to move to a dual-band collection strategy in the future, provided reasonable SNR can be achieved for both fluorescence collection bands.

3. Experimental technique

3.1. *Expansion tube and test gas conditions*

Toluene PLIF thermometry is demonstrated on supersonic flows generated in the Stanford Expansion Tube Facility. An expansion tube consists of three sections of concentric tube, separated by dividers known as diaphragms (Figure 6). Test gas conditions are determined by the relative fill pressures and species in each of the three sections. The test gas, the gas in the driven section, is first processed by a shock and then by an unsteady expansion to its final state T_5, P_5, and M_5. The state 5 test gas flows through a $30 \times 30 \times 30$ cm test section, which has optical access via fused-silica windows on three sides. See Heltsley *et al.* (2006) for a thorough description of the facility and its operation.

A 12 L mixing tank is used to seed 0.5% toluene by volume in a balance of nitrogen; this mixture is the test gas. The tube is initially filled with test gas (toluene in nitrogen) at 491.2 mbar, driver gas (helium) at 18.6 bar, and expansion gas (helium) at 333.3 mbar.

Expected conditions can be calculated from ideal shock jump equations (Trimpi 1962) using the initial fill pressures. Ideal calculations are computed using a constant γ assump-

tion, and γ is calculated for the nitrogen-toluene mixture using NASA 9-term polynomials for c_p (McBride *et al.* 2002). Test gas conditions can also be inferred by measuring primary and secondary shock speeds M_{s1} and M_{s2} via time-of-flight shock counters, and substituting these values into the ideal shock-jump equations that describe expansion tube operation; this is referred to as the semi-empirical method. Results for the semi-empirical method can be found in Table 1, and uncertainties are reported as $\pm$ one standard deviation calculated over five expansion tube tests.

Conditions were selected such that free stream static pressures are greater than 1 bar and static temperatures are no more than 600 K, and temperatures behind the primary shock T_2 do not exceed 1000 K to ensure that toluene does not pyrolyze before the test gas reaches the test section. Furthermore, Mach number was selected to prevent post-shock temperatures from exceeding $\sim$ 800 K, so as to maximize LIF signals and SNR.

3.2. *Single-band imaging configurations*

Single-band collection imaging is implemented for imaging of supersonic flow over a wedge and a cylinder. A 266 nm light source is selected for excitation owing to its larger signal levels and greater temperature sensitivity for oblique shock thermometry. A Coherent Powerlite 8000 Nd:YAG pulsed laser is externally frequency quadrupled to 266 nm. Cylindrical lenses are used to form a 1 mm-thick light sheet that enters the test section from the top of the test section (Figure 6). The laser pulse is 10 ns in duration.

Fluorescence is captured using an Andor iStar ICCD camera with a $f/2.8$, UV lens. A Schott Glass WG280 long-pass filter is used to block reflected or scattered 266 nm light, and a UG11 short-pass filter is used to block ambient light. The laser pulse is 10 ns in duration, the camera is gated to 200 ns, and fluorescence lifetimes of toluene with 266 nm do not exceed 10 ns for the conditions investigated in this work (Faust *et al.* 2011). Images are post-processed to correct for laser sheet non-uniformity at which time a background subtraction is also performed. The imaging system has spatial resolution of 100 mm per pixel.

4. Results

4.1. *Single-band toluene PLIF thermometry using an oblique shock*

Using the method described in section 3.2, a toluene PLIF image of supersonic flow over a wedge is acquired. A hardened steel wedge with turning angle θ of 19.7° is placed in the test section. As shown in Figure 7a, the shock is clearly visualized in the image, marked by the sharp drop in signal, corresponding to an increase in temperature. The shock is 3 to 5 pixels wide (300 to 500 mm), and its width is limited by the focus and resolving power of the imaging system. The shock angle β is measured to be 46.4°, resulting in a Mach number of 2.25 using γ calculated for the test gas mixture at 500 K.

Spatial signal-to-noise ratios in LIF signal are calculated over 25×25 pixel windows throughout the image by taking the average signal value in a window divided by the RMS of signal in that window. Upstream and downstream of the shock, SNRs of approximately 25 and 15 are calculated, respectively. These SNR values are reported as approximate owing to the non-uniformity in signal evident in the image, which may result from non-uniform seeding or non-uniformities in the flow field.

The LIF signal image (Figure 7a) is converted to temperature (Figure 7b) per the method prescribed in section 2.1. To more reliably approximate S_{fu}/S_{fd} and determine

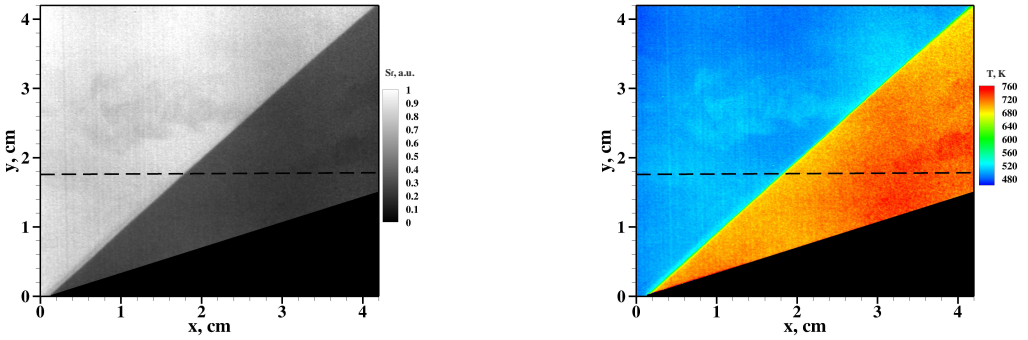

(a) (b)

FIGURE 7. Toluene PLIF signal (a) and temperature (b) images of supersonic flow over a wedge.

	P_5	T_5	M_5
Ideal	1.30 bar	579 K	2.05
Semi-empirical	1.30 ± 0.02 bar	515 ± 2 K	2.16 ± 0.2
Measured (PLIF)	-	501 ± 19 K	2.25

TABLE 1. Comparison of ideal, semi-empirical, and measured test gas conditions

the location of the oblique shock, an error function of the following form is fit across the shock:

$$y = A + B * erf(C \times (x - x_{shock})), \tag{4.1}$$

where A, B, C, and x_{shock} are fit parameters. This error function is fit over a 30 pixel window across the shock, and the first and last points of the fitted error function are used to calculate the signal ratio S_{fu}/S_{fd}. The reference temperature T_{cal} in Equation 2.2 is taken as the average temperature T_u inferred along the upstream edge of the shock, and is found to be 501 K. Figure 8a shows a representative signal profile across the image is (taken along the dotted line in Figure 7).

For values reported in Table 1, uncertainties reported for the semi-empirical results are ± 1 standard deviation calculated from five separate expansion tube shots. Calculating uncertainty in temperature using Equation 2.8 for single-band imaging, using $SNR_1 = 25$ and $SNR_2 = 15$, we obtain an uncertainty in temperature dT of approximately ± 19 K at 501 K and ± 22 K at 725 K, these uncertainties are plotted as error bars in Figure 8b at $x = 1$ cm and $x = 3$ cm.

The disagreement in T_5 between ideal theory (579 K), the semi-empirical method (515 K) , and PLIF measurement (501 K) can be attributed to the deficiencies in the model describing expansion tube operation; the ideal equations neglect viscous effects, such as boundary layer growth and transition in the expansion tube, as well as non-idealities in diaphragm rupture. Furthermore, the effects of the filters (WG280 and UG11)

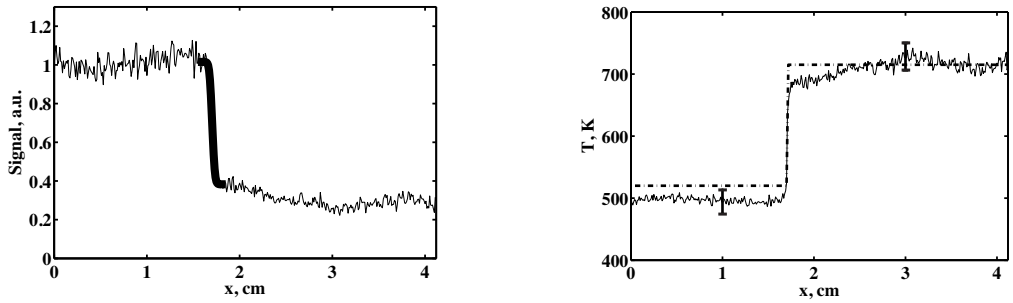

(a) (b)

FIGURE 8. (*a*) Signal along dotted line in Figure 7. Bold line near shock indicates region over which the error function (Equation 4.1) is fit. (*b*) Inferred temperature (*solid*) and expected temperature (*dash-dot*) from ideal oblique shock relations.

on the calibration curve of Figure 2a have not been considered for single-band toluene thermometry.

4.2. *Single-band imaging of supersonic flow over a cylinder*

Single-band toluene PLIF imaging is performed similarly as described in section 3.2 to visualize the flow field around a cylinder in supersonic cross flow. An aluminum cylinder of diameter $D = 19$ mm (0.75") is mounted in the test section and subjected to the same nominal flow conditions as described in section 3.1. The shock is again visualized by a sharp drop in signal. Similar SNR values are achieved as for the wedge: approximately 25 and 12 upstream and downstream of the shock, respectively.

A companion 2D, steady, inviscid, variable γ simulation of a nominally identical flow configuration has been computed using FLUENT. Half of the flowfield is meshed using a hexahedral unstructured grid containing approximately 25000 cells; a symmetry boundary condition is imposed along the edge intersecting the diameter of the cylinder. The fluid is modeled with a variable γ ideal gas, with a fifth-degree polynomial-fit computed for γ of a 99.5% nitrogen/0.5% toluene mixture from 400 K to 1000 K using the NASA 9-term polynomial (McBride *et al.* 2002). The mesh extends $5D$ upstream, downstream, and vertically from the cylinder. An implicit second-order upwind solver is implemented, and grid convergence has been established by computing the solution on a twice coarser grid (not shown).

The experimental PLIF image is plotted in the top half of Figure 9a; the synthetic PLIF signal, computed from the LIF model of Equation 2.1 with σ and ϕ from Figure 1, is displayed in the bottom half of the same figure. The inflow Mach number in the computation was iterated to match the bow shock standoff distance given by the simulation to what was observed in the experiment. The Mach number required to meet this condition is $M = 2.33$.

The synthetic PLIF signal is normalized by the expected signal at 501 K and 1.3 bar, the free stream temperature and pressure. The experimental PLIF image is normalized by the average signal upstream of the shock (S_{fcal}). In both images, we can clearly identify the shock by a steep drop in signal. A streamline (*white line*) has been plotted in the computation and at the corresponding location in the experimental PLIF image. Along this streamline, signal as well as temperature and pressure (relative to their free stream values) have been plotted in Figure 9b. Throughout the image, we see a discrepancy in

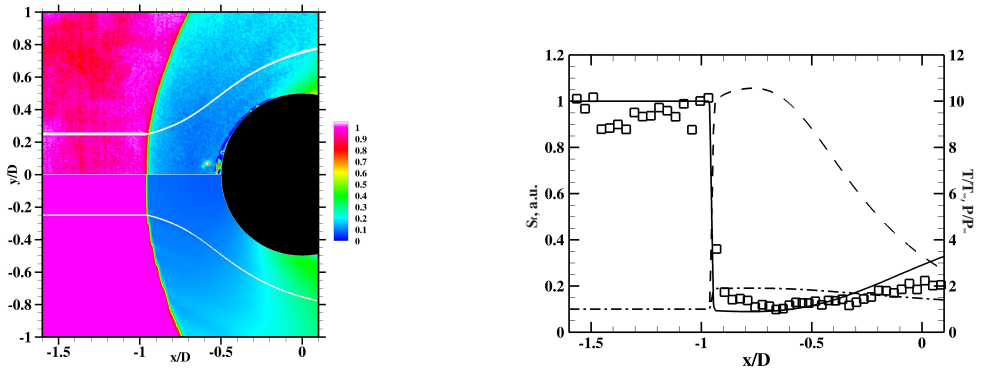

(a) (b)

FIGURE 9. (*a*) Experimental toluene PLIF image of flow over a cylinder (top half) and synthetic LIF signal (bottom half) of the same flow condition. White lines follows streamlines computed from the CFD. (*b*) Synthetic LIF signal (*solid*) experimental LIF signal (*squares*) along streamlines plotted in figure (*a*) on left ordinate. $^{P}/_{P_\infty}$ (*dash*) and $^{T}/_{T_\infty}$ (*dash-dot*) on right ordinate.

simulated versus experimental LIF signal of approximately 10% near $-1.5\frac{x}{D}$ and $0\frac{x}{D}$, but good agreement in signal ratio across the shock. The discrepancy can potentially be attributed to non-uniformities in the test gas flow or tracer seeding, an oversimplified toluene PLIF model, or viscous effects near the separation point. However, the measured signal tracks the synthetic signal through a region of highly varying temperature and pressure, illustrating the utility in single-band toluene PLIF imaging to investigate the details of complex supersonic flowfields.

5. Conclusions

A toluene PLIF thermometry diagnostic has been presented for temperature imaging of high-speed, compressible flows in an expansion tube. Single- and dual-band thermometry schemes have been described, and the accuracy of each scheme has been assessed. Single-band collection has been applied to image supersonic flow over a wedge and a cylinder. Using the ideal temperature and pressure ratios across an oblique shock, temperature has been inferred in the entire imaged field; a synthetic LIF signal for the flow over the cylinder has been computed from a 2D, inviscid simulation of the flow, and it has been compared to the corresponding experimental LIF image. Good agreement between theory and measurement were observed for both cases.

Further work is required to developed the technique for single-wavelength excitation/dual-band collection imaging in order to make the approach a robust thermometry diagnostic in flowfields with nonuniform tracer seeding and pressure distribution and take full advantage of the technique in more general high-speed flow configurations of interest.

Acknowledgements

This is based upon work supported by the Department of Energy under the Predictive Science Academic Alliance Program (PSAAP) at Stanford University, Award Number(s) DE-FC52-08NA28614. The authors would like to thank Khadijeh Mohri of Universität Duisburg-Essen for her assistance. The authors would also like to thank Jon

Koch, Wieland Koban, and Christof Schulz for the toluene emission spectra data they graciously provided.

REFERENCES

Burton, C. S. & Noyes, W. A. 1968 Electronic energy relaxation in toluene vapor. *J. Chem. Phys.* **49** (4), 1705–1714.

Cheung, B. 2011 Trace-based planar laser-induced fluorescence diagnostics: Quantitative photophysics and time-resolved imaging. PhD thesis, Stanford University.

Faust, S., Dreier, T. & Schulz, C. 2011 Temperature and bath gas composition dependence of effective fluorescence lifetimes of toluene excited at 266 nm. *Chem. Phys.* **383** (1-3), 6 – 11.

Heltsley, W. N., Snyder, J. A., Houle, A. J., Davidson, D. F., Mungal, M. G. & Hanson, R. K. 2006 Design and characterization of the stanford 6 inch expansion tube. In *42nd AIAA/ASME/SAE/ASEE Joint Propulsion Conference & Exhibit*. Sacramento, California.

Koban, W., Koch, J. D., Hanson, R. K. & Schulz, C. 2004 Absorption and fluorescence of toluene vapor at eleveated temperatures. *Phys. Chem. Chem. Phys.* **6** (2940-2945).

Koban, W., Koch, J. D., Hanson, R. K. & Schulz, C. 2005*a* Oxygen quenching of toluene fluorescence at elevated temperatures. *Applied Phys. B: Lasers Optics* **80**, 777–784.

Koban, W., Koch, J. D., Hanson, R. K. & Schulz, C. 2005*b* Toluene LIF at elevated temperatures: implications for fuel-air ratio measurements. *Applied Phys. B: Lasers Optics* **80**, 147–150.

Koch, J. 2005 Fuel tracer photophysics for quantitative planar laser-induced fluorescence. PhD thesis, Stanford University.

McBride, B. J., Zehe, M. J. & Gordon, S. 2002 NASA glenn coefficients for calculating thermodynamic properties of individual species. *Tech. Rep.* TP-2002-211556. NASA.

Mohri, K., Luong, M., Vanhove, G., Dreier, T. & Schulz, C. 2011 Imaging of the oxygen distribution in an isothermal turbulent free jet using two-color toluene LIF imaging. *Applied Phys. B: Lasers Optics* **103**, 707–715.

Schulz, C. & Sick, V. 2005 Tracer-LIF diagnostics: quantitative measurement of fuel concentration, temperature and fuel/air ratio in pratical combustion systems. *Progress Energy Combust. Science* **31**, 75–121.

Trimpi, R. L. 1962 A preliminary theoretical study of the expansion tube, a new device for producing high-enthalpy short-duration hypersonic gas flows. *Tech. Rep.*. NASA.

Yoo, J., Mitchell, D., Davidson, D. F. & Hanson, R. K. 2010 Planar laser-induced fluorescence imaging in shock tube flows. *Exp. Fluids* **45**, 751–759.